

The Characteristics of Large Area Processing Plasmas

Sea Eun Park, Byung Ug Cho, Jae Koo Lee, *Member, IEEE*, Young Joon Lee, and Geun Young Yeom

Abstract—In order to improve production efficiency, large-diameter wafer substrates (300-mm diameter) and large-area glass substrates (from 400 cm² to 1 m²) have been adopted recently. As a result, the development of large and high-density plasma source has become essential. To investigate the discharge phenomenon in the chamber that consists of embedded antenna coil in the rectangular system (1020 × 830 × 437 mm), we have developed a two-dimensional fluid simulation model. In order to check our model, the results from our simulation have been compared with available experimental data. The comparison is generally in a good agreement with experiments. Depending on the current direction and powered method, the distribution of plasma parameters has many differences. In our simulation with a chamber larger than is usually used in other experiments, we examine three effects: the distance between antenna coils, structure in the chamber, and the depth of the chamber. The parameters, which affect nonuniformity, electron temperature, and others, can be explained in a manner similar to the inductively coupled plasma source with a cylindrical chamber. Our simulation results confirm that the embedded antenna coil system with a suitable environment can be extended by many antenna coils as a large-area plasma source.

Index Terms—Embedded antenna coil, inductively coupled plasma source, large-area plasma source.

I. INTRODUCTION

INDUCTIVELY coupled plasma source is widely used for high-density plasma etching in semiconductor processing with low gas pressure. In this system, plasma is generated by induced magnetic and electric fields inside the radio frequency (RF)-driven cylindrical coil. The common feature of this system is that the RF or microwave power is coupled to the plasma across a dielectric window or wall rather than by direct connection to electrode in the plasma, as is the case in capacitive discharge. In recent years, in order to improve production efficiency, large-diameter wafer substrates (300-mm diameter) and large-area glass substrates (from 400 cm² to 1 m²) have been adopted. As a result, the development of large and high-density plasma has become essential. When the common inductively coupled plasma is used as a large plasma source, several problems can be encountered. First, azimuthal nonuniformity may arise because of the standing wave effect. Second, induced voltage is higher over the large area, and the capacitive coupling increases. Third, in order to produce plasma with large area and sustain high pressure, large and very thick dielectric material must be used. However, it is not only difficult to use but

also expensive, and power transfer efficiency is poor. In order to overcome these problems, several researchers have proposed the new large-area plasma source. Chen *et al.* [20] proposed a helicon plasma source with seven tube array in large dc magnet or individual permanent magnet that achieved 3% uniformity in 400-mm-diameter area. Meger *et al.* [21] obtained plasma that is generated by a sheet electron beam with voltages and current densities of the order of kilovolts and tens of milliamps per centimeter squared and the area of the test system 1000 × 1000 mm. Lieberman *et al.* [1]–[3] made a rectangular chamber that consists of 8-rod embedded antenna and obtaining 3.5% uniformity in 360 × 465 mm processing area. We are investigating a chamber (1020 × 830 × 437 mm) larger than the one used by Lieberman *et al.*. This chamber consists of 19 quartz tubes for antenna coil and 18 quartz tubes for other elements. Moreover, the processing area is 730 × 920 mm. In order to investigate the discharge phenomena in that system, we have developed a two-dimensional (2-D) fluid code in the cartesian coordinate according to the experimental geometry. The modeling and simulation of large-area plasma source were studied using the fluid code. The results of the simulation are presented in [10]. However, the present model has several differences, and this simulation is performed in a large-area domain unlike the previous work. The difference of the recent model from previous one is explained in Section II. Our model is based on the solution of transport equation (continuity and momentum transfer equation in drift-diffusion approximation). Potential is calculated from Poisson's equation. Three momentums derived from the Boltzmann equation are used for particles. However, the energy equation is excepted for ion. Using this code, we analyze plasma density and temperature by varying three parameters: distance between antenna coil, structure in a chamber, and the depth of the chamber. An inductively coupled plasma source has two modes, which are the capacitive discharge due to voltage of the antenna coil and the inductive discharge due to the induced field. The finite-difference method (FDM) is used in this model, with the same grid size for all grids. Therefore, mapping the simulation domain, we obtain a size smaller than the experimental system size. Our simulation does not follow the exact chamber dimensions (1020 × 830 × 473 mm). The difference, however, is very small.

II. MODEL DESCRIPTION

There are many ways studying plasma using computer simulation, among which kinetic, fluid, particle-in-cell (PIC), and hybrid simulation [13] are worth mentioning. The kinetic model directly solves the Boltzmann equation in proper dimension and velocity space. It can provide more information than a fluid model because it does not use any assumptions. However, this method is computationally very intensive and requires more

Manuscript received October 20, 2002; revised February 12, 2003. This work was supported by the Korea Ministry of Science and Technology under the National Research Laboratory Program.

S. E. Park, B. U. Cho, and J. K. Lee are with the Department of Electronic and Electrical Engineering, Pohang University of Science and Technology, Pohang 790-784, South Korea (e-mail: jkl@postech.ac.kr).

Y. J. Lee and G. Y. Yeom are with the Department of Materials Engineering, Sungkyunkwan University, Suwon, Gyeonggi 440-746, South Korea.

Digital Object Identifier 10.1109/TPS.2003.815247

computation time compared to the fluid model. We have developed 2-D fluid codes (FL2D and FL2P) that can be used for modeling capacitively coupled plasma sources [10], [16] and plasma display panels [9], [11], respectively. In order to simulate inductively coupled plasma source equipment, we have improved on the 2-D fluid code for cylindrical and cartesian coordinates (FL2I). In this paper, the model for cartesian coordinate is used. This model consists of a set of fluid equations for electron and ion (Ar^+), solved self-consistently with Poisson's equation. The ground state Ar atom density is fixed according to a specified neutral pressure and is spatially uniform. Ion temperature is assumed to be equal to that of neutral species. Under these assumptions, the model equations can be written as

$$\frac{\partial n_j}{\partial t} + \nabla \cdot \mathbf{\Gamma}_j = R_{iz} \quad (1)$$

$$\nabla^2 V = \frac{e}{\epsilon_0} (n_e - n_p) \quad (2)$$

$$\mathbf{\Gamma}_j = -D_j \nabla n_j + \text{sgn}(q_j) n_j \mu_j \mathbf{E} \quad (3)$$

$$\frac{\partial}{\partial t} \left(\frac{3}{2} n_e k T_e \right) + \nabla \cdot \mathbf{\Gamma}_e + e \nabla \cdot \mathbf{E} + P_{\text{coll}} = P_{\text{in}} \quad (4)$$

$$\mathbf{q}_e = -\frac{5}{2} n_e D_e \nabla (k T_e) + \frac{5}{2} k T_e \mathbf{\Gamma}_e \quad (5)$$

$$\nabla^2 E_z(x, y) + \frac{\omega^2}{c^2} K E_z(x, y) = -j \omega \mu_0 J_z \text{ext} \quad (6)$$

$$P_{\text{abs}} = \frac{1}{2} \text{Re}(\sigma |E_z(x, y)|^2). \quad (7)$$

Equation (1) is the continuity equation, and n_j and $\mathbf{\Gamma}_j$ are the number density and the flux of species j , respectively. The continuity equation is integrated by a Douglass and Gunn alternative direction implicit (ADI) method [15]. The source term R_{iz} is given in the following form (see Stewart *et al.* [4]):

$$R_{iz} = n_e n_N K_{iz} \quad (8)$$

where n_N and K_{iz} are the neutral gas density and the ionization rate coefficient, respectively. Equation (2) is Poisson's equation for electrostatic field E .

Equation (3) is the first momentum transfer equation in drift-diffusion approximation. It is solved by using the Sharfetter-Gummel scheme [14], which supports large density gradients. Mobility μ_j and diffusion coefficient D_j are obtained from the Einstein relation. Ion-neutral collision frequency is constant because ion temperature does not change. Mobility for electron and rate coefficients for electron-neutral collisions are functions of electron temperature. Makabe *et al.* [24], [25] use the function of E/N from database for this swarm parameter. Equation (4) is the energy balance equation for electrons. P_{coll} is the energy loss rate per unit volume due to the electron-neutral collisions [4], [5]. It can be expressed as

$$P_{\text{coll}} = n_e n_N \sum_j K_j \epsilon_j \quad (9)$$

$$K_j(T_e) = \sigma_j v_e(T_e) \exp\left(\frac{-\epsilon_j}{k T_e}\right) \quad (10)$$

where the constants σ_j and ϵ_j are the same in [4]. P_{in} and ϵ_j are the energy gain rate per volume due to the external source and

the energy loss per electron per collision of type “ j ,” respectively. Equation (5) is the energy flux, which is written in the form similar to that of fluxes of charged particles using the exponential scheme proposed by Shaffetter and Gummel [14]. Equation (6) is a complex wave equation for induced electric field in z direction E_z has zero value on the conductor surface. σ_p and K are plasma conductivity and cold plasma dielectric tensor

$$K = 1 + \frac{j}{\omega \epsilon_0} \sigma_p \quad (11)$$

$$\sigma_p = \frac{\epsilon_0 \omega_{pe}^2}{v_{en} - j \omega}. \quad (12)$$

The period averaged inductive power is given by (7) [6]. In [10], the power deposition was given by the expression: by $P = P_0 \exp(-2x/\delta)$, where $\delta = (m_e/e^2 \mu_0 n_e \omega)^{1/2}$, and P_0 (in units of $\text{W} \cdot \text{cm}^{-1}$) was adjusted to yield the total power as prescribed in the input parameter. However, self-consistent calculation of the induced electric field is adopted in the present paper analogous to [7] and [8]. At the initial state, we obtain the solution of the wave equation and power deposition from the temporary coil current. Then, at the end of calculation, the coil current is scaled to yield the specified power deposition because the coil current is proportional to the square root of the power deposition [17]. At the next step, a new solution of the wave equation is obtained by the scaled current, and solved by the successive over-relaxation (SOR) algorithm with Chebyshev acceleration.

The substitution of (3) into (2) gives [7]

$$\nabla \cdot \left[\left(\epsilon + \sum_j \Delta t n_j \mu_i \text{sgn}(q_j) \right) \mathbf{E} \right] = \sum_j (q_j n_j + \Delta t \nabla \cdot (D_j \nabla n_j)). \quad (13)$$

The modified Poisson's (13) is solved by the same numerical method which is used for the wave equation [9].

Particle fluxes to boundary surface are calculated as [9], [12]

$$\mathbf{\Gamma}_p \cdot \mathbf{n} = \text{sgn}(q_p) s_p \mu_p n_p \mathbf{E} \cdot \mathbf{n} + n_p \frac{\bar{v}_p}{4} \quad (14)$$

$$\mathbf{\Gamma}_e \cdot \mathbf{n} = -s_e \mu_e n_e \mathbf{E} \cdot \mathbf{n} + n_e \frac{\bar{v}_e}{4} + \mathbf{\Gamma}_{se} \cdot \mathbf{n} \quad (15)$$

$$\mathbf{\Gamma}_{se} = - \sum_p \gamma_{se,p} \mathbf{\Gamma}_p. \quad (16)$$

Here, γ and \bar{v} are the secondary electron coefficient by ion and mean velocity, respectively. The symbol s is defined in such a way that it is nonzero ($s = 1$) only if the drift velocity is directed toward the wall. Otherwise $s = 0$.

III. SIMULATION RESULTS

A. Comparison With Experimental Results

Fig. 1 shows whether or not the embedded antenna coil is extended as large area plasma source ($798 \times 798 \times 140$ mm). High and uniform plasma density appears near the antenna with an increasing number of antenna coil. However, in case of larger distance between antenna coil, high-density plasma appears in

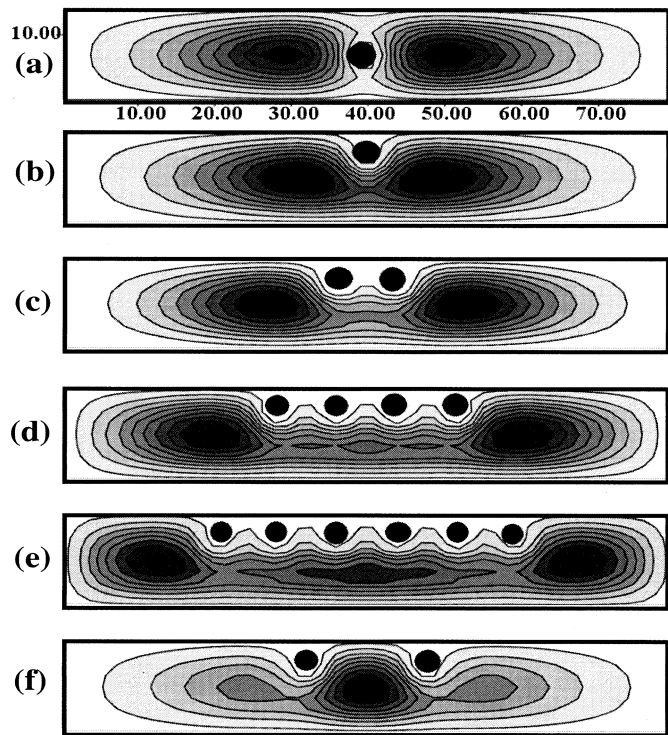


Fig. 1. In the system (vertical length (x) (x) = 792 mm, depth (y) = 140 mm): (a) Ar^+ density with one antenna coil at center position; (b) with one antenna coil; (c) with two antenna coils; (d) four antenna coils; (e) six antenna coils upper position ($y = 100$ mm); and (f) the distance antenna coil is twice than (c).

the region, as shown in Fig. 1(f). In order to obtain uniform density, a suitable distance must be found. Thus, we investigated three effects in a chamber (vertical length = 830, horizontal length = 1020, depth = 437 mm) bigger than that in [1]. This problem and its effects will be discussed in Section III-B. Wu and Lieberman [1] experimentally showed that plasma density profile can be influenced by power dissipated in the system [1]. In order to confirm our model and investigate the plasma phenomenon, we compared our results with the experiment. The plasma source used in [1] was a $710 \times 610 \times 200$ mm metal chamber providing a processing area of 370×470 mm for large-size wafers and glass substrates for flat-panel displays. In the experiment, a tuning network was used to launch a traveling wave. In our simulation, we assume that the absolute value of the current is the same on all antennas, and the voltage of antenna coil is not considered. Fig. 2 shows the ion density for different values of power and pressure (type 4 in Fig. 3). The density minimum is in the middle position analogous to experimental results [1]. The magnitude and distribution of density are the same as in Fig. 8 from [1]. Fig. 2(c) and (d) shows that the profile of the induced electric field affects power deposition. The induced electric field at any position is calculated as the sum of induced electric fields of each current. The induced electric fields of adjacent currents have greater influence than that of currents far from the position. Thus, the induced electric field is zero nearly the center between antenna coils. It can be clearly seen if we consider one side view of the simulation domain, the current changes its direction, as shown in Fig. 3 (type 4). Fig. 3 shows the scheme for four types that consist of serpentine and parallel connection. If

the antenna coil has parallel connection of type 3, E_z field appears as the sum of each induced electric fields over the region between the antenna coil because the current directions of two sources are the same, as shown in Fig. 4. Therefore, the electron temperature and density for parallel connection are higher than that of series connection. The effect of localized heating near the powered quartz tube is clearly evident from the electron temperature distribution which has a peak near the quartz tube. However, the electron temperature near the powered quartz tube has a different distribution as a powered method (Fig. 4). Density profile is not exactly the same as the power deposition profile or electron temperature. At the initial time step, the density profile is similar to that of power deposition. However, it changes with time as shown in Fig. 4. Electron temperature and plasma density have rough distribution for type 2. Thus, in this system with the nonuniform distance between the antenna coil, it is difficult to control plasma parameters and to obtain good uniformity (Fig. 4). For type 3, when we consider the standing wave effect, the current path is reduced with subsequent reduction in the current and voltage. As a result, the best uniformity can be obtained for the coils of type 3. If eight rods have parallel connections, the sum of the induced electric fields will have a mount shape. Therefore, the density distribution will have the same shape. Fig. 5 shows Ar^+ density and electron temperature that are obtained for type 3 shown in Fig. 3. As the pressure increases, Ar^+ density increases and concentrates around four sets. Electron temperature decreases because of enhanced collision processes. At high pressure, more localized heating in the high-field region is observed with a shorter electron relaxation length. These factors explain the roughness of the density profile at high pressure. We compared our results with [2] where oxygen has been used. We consider that generally, the plasma density of Ar discharge is higher than that of oxygen [7], [22], [23]. Our simulation result shows the same tendency.

B. Effect of Distance Between Antenna Coil

To design an embedded antenna chamber, we have to know the optimized distance between antenna coils. As it was mentioned earlier, if the standing wave effect is taken into consideration, the decrease of the total length of antenna coil leads to a better density uniformity. In other words, the distance between antenna coil has to be increased. However, when we assume that the current difference in the line source does not exist, then, the effect of the distance is distinguished from the former case. We used the simulation domain which is $798 \times 798 \times 140$ mm. As mentioned previously, the vertical length can not be exactly 830 mm, and a shorter depth length has been used. Thus, we have the simulation domain with vertical length = 798 and depth = 140 mm. The antenna plane is 4 cm away from left side, and the substrate is about 10 cm away from the antenna plane. The distance between adjacent antenna coil is varied in the range from 72 to 132 mm. The pressure and power is 5 mtorr and 1000 W, respectively. In order to compare the effect on the fixed domain, the numbers of antenna coils were decreased with the increase of the distance. Fig. 6 shows the contours of the Ar^+ density. The peak density appears near the side wall. As the distance increases, the peak position of density occurs at the region between antenna coils, and the magnitude of the peak density and

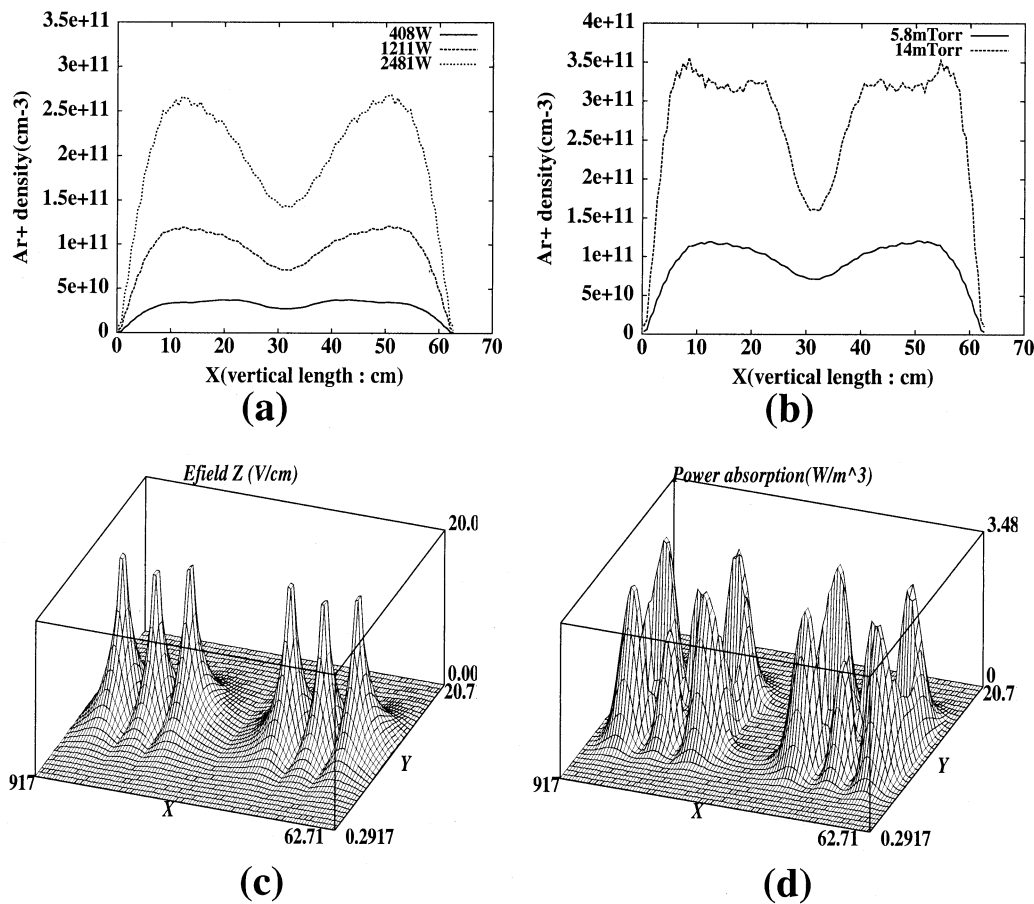


Fig. 2. Ar^+ density profile: (a) for different powers; (b) for different pressures at $d = 4.75$ cm; (c) $|E_z|$ for type 4; and (d) power absorption for type 4, where d is the distance from antenna plane.

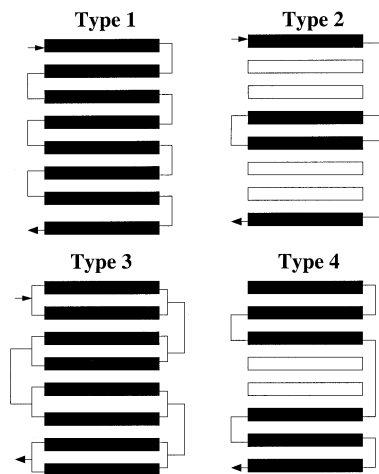


Fig. 3. Type 1—serpentine connection. Type 2—serpentine connection with empty quartz tube. Type 3—series path with four sets of parallel connection. Type 4—six rods powered with the middle two rods unpowered.

nonuniformity increase. Electron temperature near the substrate decreases. Fig. 7 shows Ar^+ density, nonuniformity at positions $d = 4.75$ cm and $d = 9.75$, and electron temperature near the substrate (d is the position with respect to the antenna plane). As a result, the effect of diffusive loss due to quartz tube is smaller than that for the small distance. Therefore, if the distance between adjacent antenna coil is larger, the density profile is dis-

tributed analogous to the antenna pattern, as shown in Fig. 7(a), where the density for positions $d = 4.75$ and $d = 9.75$ cm is presented. For $d = 9$ and $d = 9.75$ cm, nonuniformity is satisfactory (2.9%). If the position of the substrate is close to the antenna plane, the system with a shorter distance between antenna coil is a good candidate for large-area plasma processing source. In the opposite case, longer distance allows a good uniformity with low electron temperature. In other words, in order to obtain good uniformity in the system with a longer distance between the antenna coil to eliminate standing wave effect, the position of the substrate has to be at longer distances from the antenna plane. The simulation results presented in Figs. 6 and 7 show this tendency. The peak density is observed at the edge of antenna coil because the maximum value of the induced electric field is at the similar position. The steady-state profile in the center region is determined by the ambipolar diffusion. Stittsworth and Wendt [18] reported on the reactor geometry and plasma uniformity in a planar inductively coupled radio frequency argon discharge. When λ_e is short compared to the radius of maximum electron heating, then the energy of the energetic electron will be spent in ionization before they reach the discharge axis. Energy relaxation length λ_e is defined as

$$\lambda_e = \sqrt{\frac{\lambda_m \lambda^*}{3}} \quad (17)$$

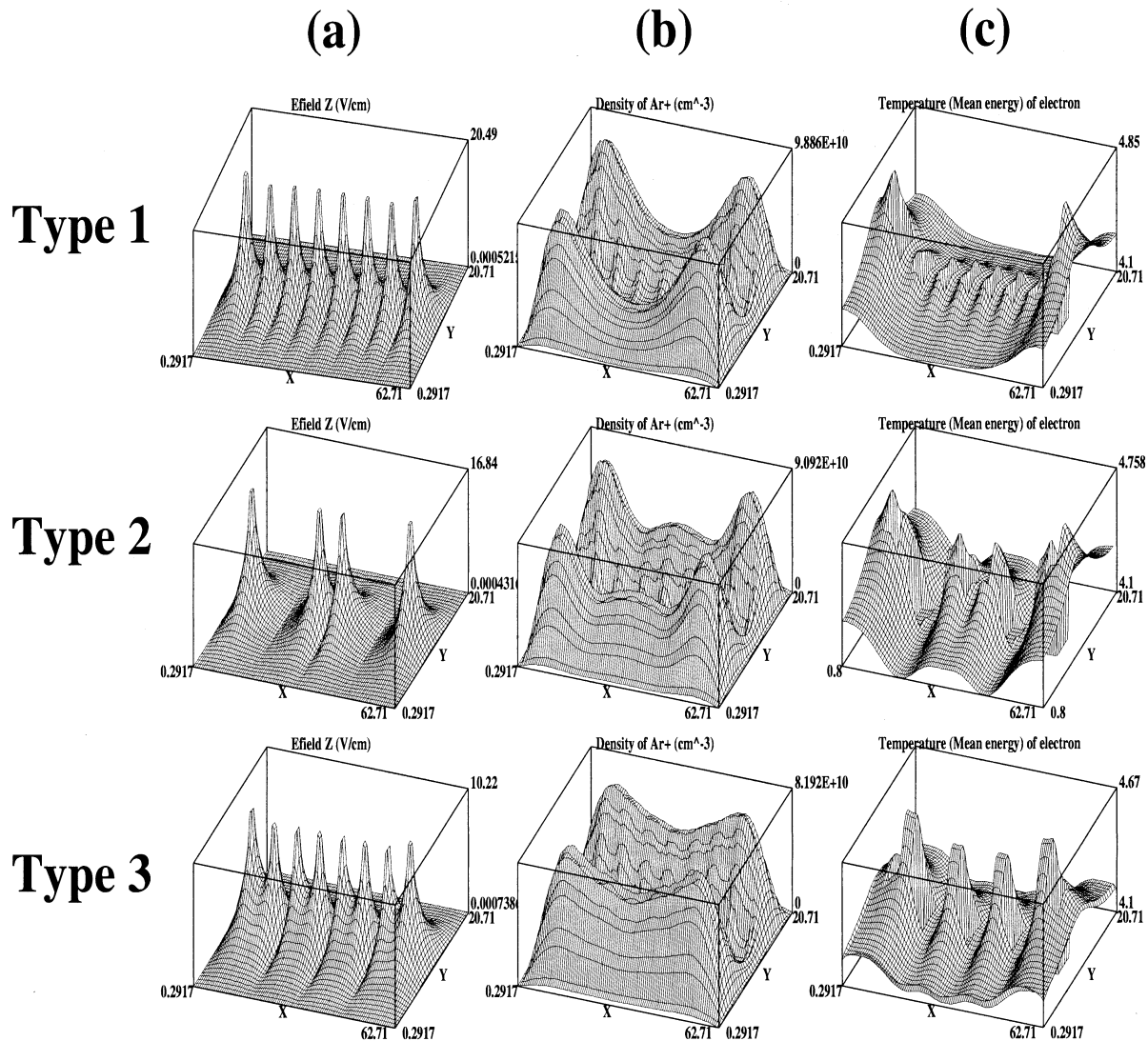


Fig. 4. (a) $|Ez|$. (b) Ar^+ density. (c) Electron temperature for type 1, type 2, and type 3 at pressure 5 mtorr and power 1000 W.

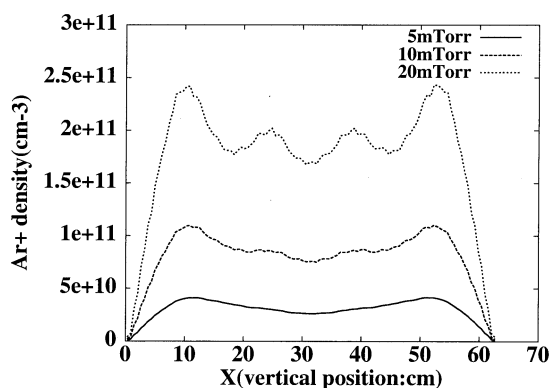
where λ_m and λ^* are the electron mean free paths for momentum transfer and inelastic collisions, respectively. If we assume that R_E and L are the distance between the edge of antenna and the center position and between antenna plane and substrate, respectively, λ_e (13.0 cm) for 5 mtorr is less than R_E and longer than L , ($L < R_E$). Therefore, the peak density occurs near R_E .

When we measure the density experimentally by probe, the probe position is important for analysis of this system. For example, if the measurement interval is greater than 5 cm, experimental data show good nonuniformity (less than 15%). However, the exact value is greater than 15%. The measurement interval has to be considered from the quartz tube diameter and the distance between antenna coils. Fig. 8 shows the effect of the interval between the wall and the edge antenna coil. In this simulation, the domain is extended as the interval variation (4.8–12 cm), and the distance (7.8 cm) between antenna coil is fixed. The pressure, power, and the number of antenna coils are 5 mtorr, 1000 W, and 10, respectively. As the length increases, the peak density decreases, whereas nonuniformity

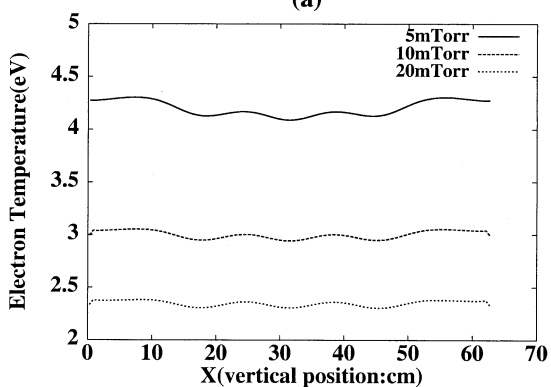
has a critical point rather than a constant variation trend of increase or decrease. The electron temperature in the total region has a change in the range from about 3.8 to 4.5 eV. In the region between the wall and the antenna coil, the density is relatively high in the range from 4.8 to 9.6 cm and low in range from 10.8 to 12 cm. The distribution of electron temperature in the bulk region is more uniform at the interval 10.8 cm than others. Therefore, the case of interval 10.8 cm has the least nonuniformity (3.6%). The result shows that choice of appropriate interval between the wall and antenna coil is very critical for uniformity as well as the total number of antenna coils.

C. Effect of Structure

To show the effect of quartz geometry, we have two different simulation domains. One consists of ten quartz tubes and ten antenna coils, the other consists of five empty quartz tubes and five quartz tubes with five powered antennas, as shown in Fig. 10. The peak density for the second simulation domain is lower than that for the first, whereas the nonuniformity for the second



(a)



(b)

Fig. 5. (a) Ar^+ density and (b) electron temperature on $d = 5$ cm in type 3, where d is the distance from the antenna plane.

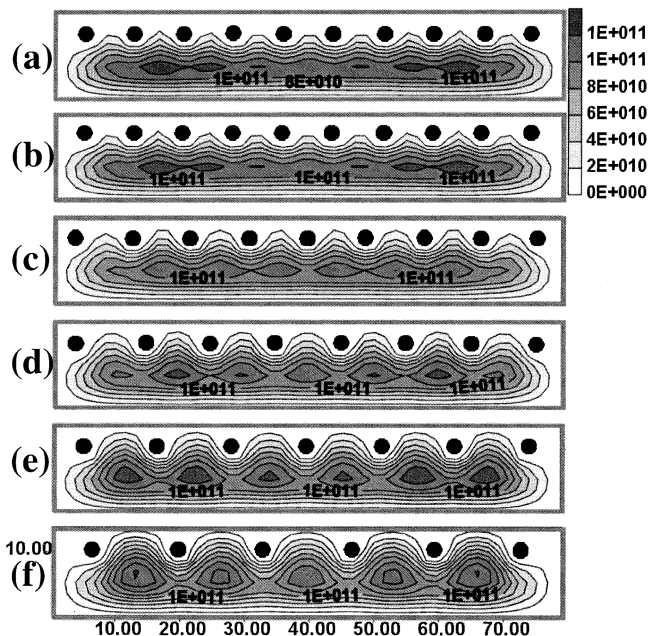
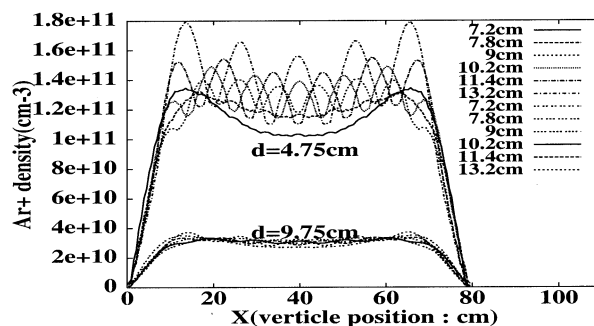
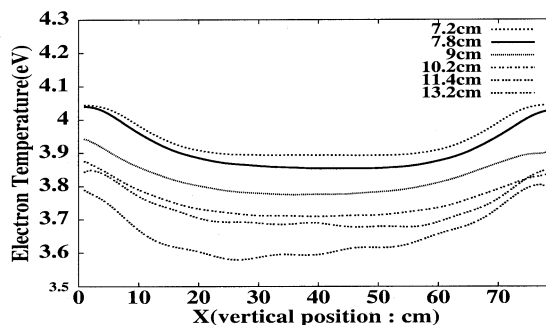


Fig. 6. Ar^+ density contour for the distance between adjacent antenna coil that is: (a) 7.2; (b) 7.8; (c) 9; (d) 10.2; (e) 11.4; (f) 13.2 cm on power 1000 W and pressure 5 mtorr.

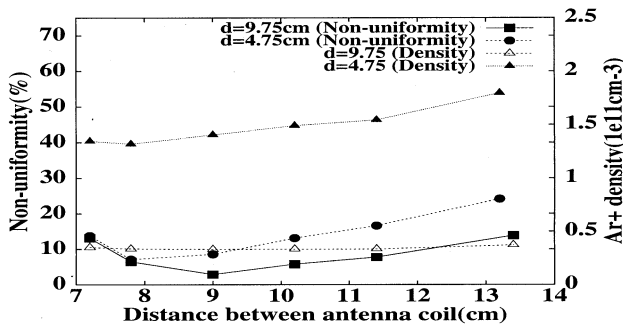
simulation domain (7.4%) is similar to that for the first (7%). Though the power deposition is different, the density profile for two cases is similar, except for the magnitude. In Section III-B, we showed the tendency of increase of nonuniformity with the increase of distance between the powered antenna. However, in



(a)



(b)



(c)

Fig. 7. (a) Ar^+ density (cm^{-3}) on vertical line. (b) Electron temperature on vertical line. (c) Nonuniformity versus distance between antenna coils.

this simulation, with the distance of 15.6 cm between two adjacent powered antenna coil, the tendency is not observed. As a result, we can conclude that the structure affects nonuniformity to a greater extent than the powered antenna source. In conclusion, if the empty quartz tube and the quartz tube with powered antenna are mixed instead of using many powered antenna coils, the difference in voltage or current due to long length antenna can be reduced practically, and lower nonuniformity can be obtained.

D. Effect of Depth

Stittsworth and Wendt [18] examined the effect of chamber height on plasma uniformity for a cylindrically symmetric planar inductive radio frequency (13.56 MHz) argon plasma generated with a single-turn circular loop antenna [19]. To investigate nonuniformity in dependence of the depth in line antenna coil system, this simulation domain with a depth of (300 mm) was used, longer than the one used in the previous case. As shown in Fig. 11, the density profile for the depth 300 mm (nonuniformity 3.1%) has good uniformity rather than

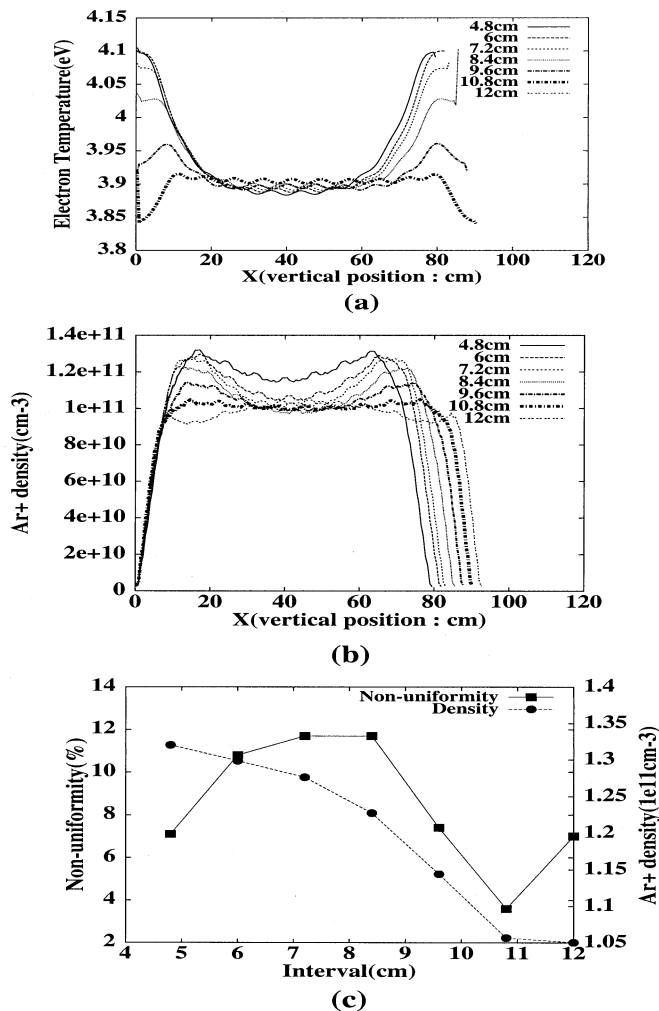


Fig. 8. (a) Electron temperature. (b) Ar⁺ density (cm⁻³) on vertical line. (c) Nonuniformity and peak density versus distance between the wall and the antenna coil.

that for the depth 200 mm (nonuniformity = 15.6%). In [18], λ_c is less than L , therefore, the position of maximum ionization is shifted toward the center. Moreover, in the embedded line antenna coil system, electron heating occurs near the quartz tubes surrounding the coil, and the induced electric field has a different magnitude because of the interference between the neighboring antenna coils. Practically, the depth affects the uniformity to a greater extent than the cylindrical system with external planar antenna coil because of the high density plasma among line antenna coils. Ar⁺ density at distances ($d = 9.5$ cm) from the line antenna coil plane is shown in Fig. 12 for the total length of line antenna coil, the length 7, 8.29, and 13.48 m. As shown in Fig. 9, the length 7, 8.29, and 13.48 m have line antennas of ten, seven, and five, in the chamber, respectively. When the distance from the antenna coil plane is 9.5 cm, the maximum density is observed. The nonuniformity as well as the maximum density is very small for this case (length = 7 m).

IV. CONCLUSION

We have developed a 2-D fluid code in the cartesian coordinate system for a large-area plasma source. In order to in-

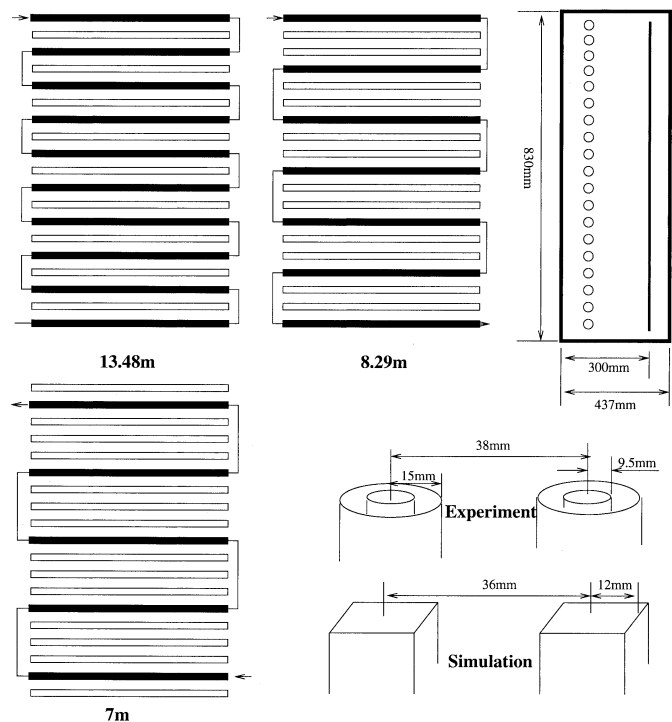


Fig. 9. (a) Ar⁺ density with ten and five antenna coils. (b) Power deposition (W/m³) with ten and five antenna coils. (c) Ar⁺ on $d = 4.75$ cm and $d = 9.75$ cm with ten and five antenna coils.

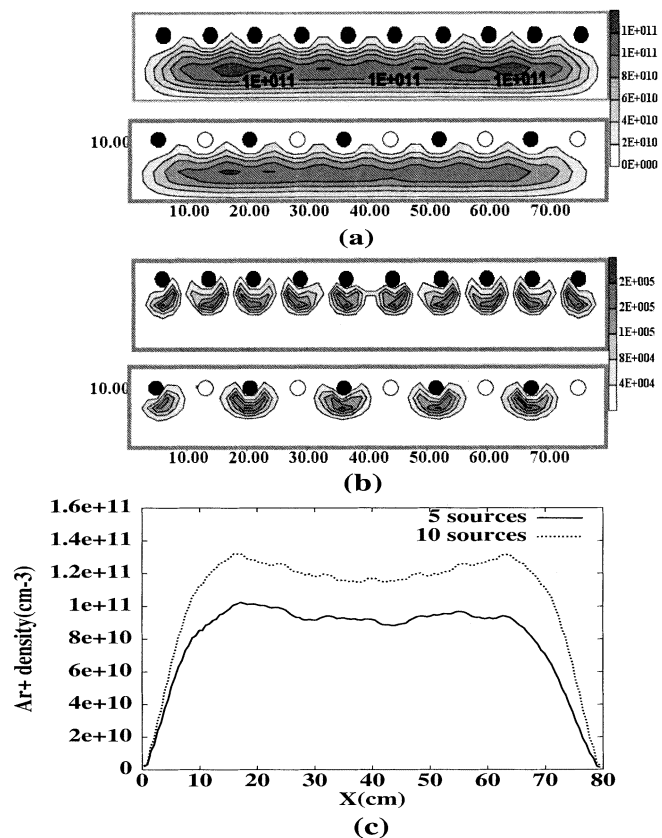


Fig. 10. Schematic diagram for the total length.

vestigate the embedded antenna coil system, the model FL2I has been used. The embedded antenna coil system can be ex-

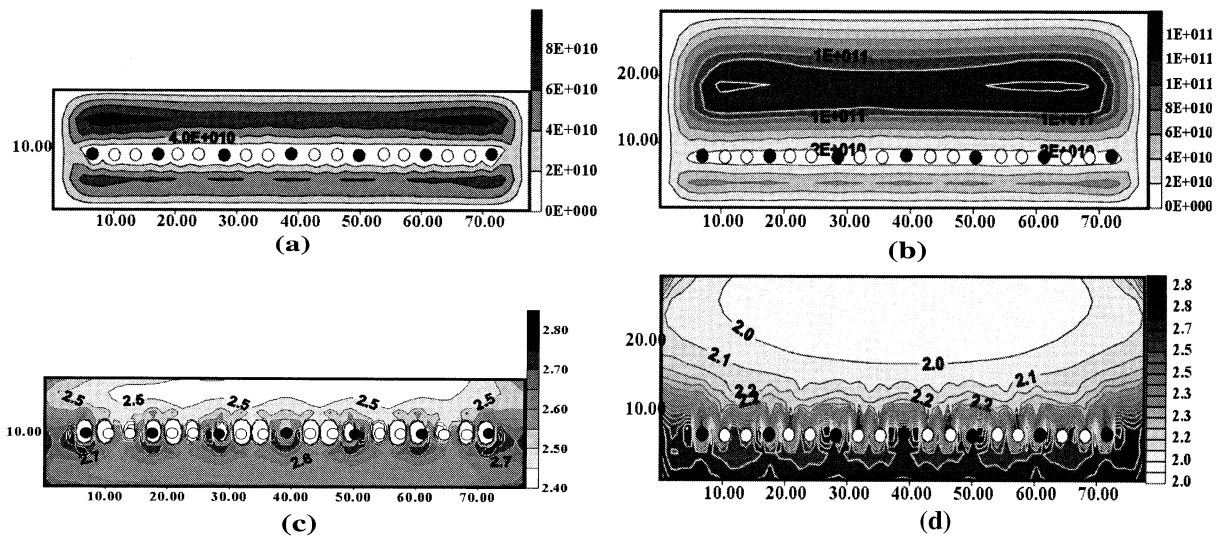


Fig. 11. (a) Ar^+ density (cm^{-3}) and (b) electron temperature (eV) in small depth (vertical length = 780 mm, depth = 200 mm, total length = 8.29 m). (c) Ar^+ density (cm^{-3}) and (d) electron temperature (eV) in long depth (vertical length = 780 mm, depth = 300 mm, total length = 8.29 m).

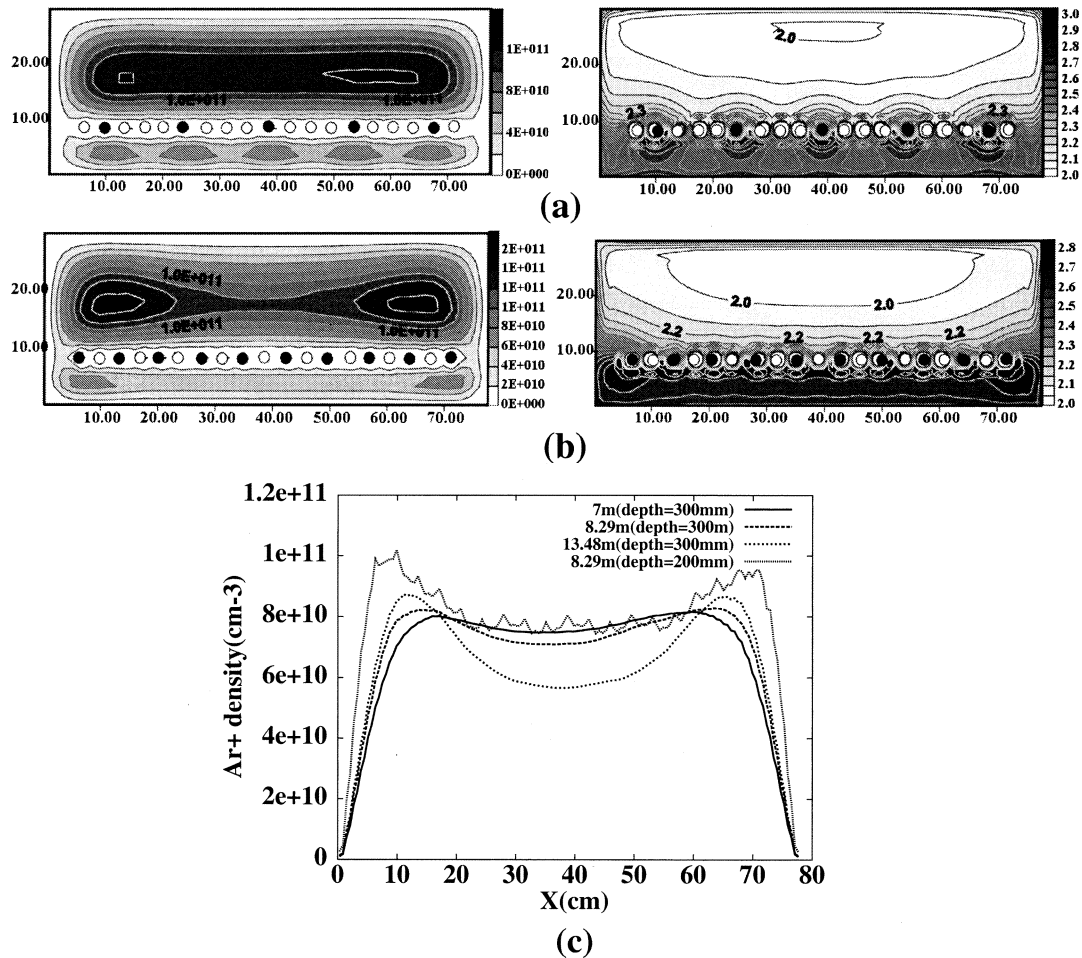


Fig. 12. Ar^+ density (cm^{-3}) and electron temperature for total antenna length (a) 7 m and (b) 13.48 m. (c) Peak density for total length 7, 8.29, and 13.48 m with depth 300 mm, and 8.29 m with depth 200 mm.

tended by many antenna coils as a large-area plasma source. Depending on the current direction of adjacent antennas, the total induced electric field can decrease or increase, which results in dissimilar patterns of power deposition and density profile. The

distance between antenna coils affects nonuniformity, electron temperature, and other plasma parameters. To make similar diffusive loss in plasma source is very important for density uniformity, and it can be obtained from empty quartz. The effect

of inner geometry on plasma nonuniformity is more profound than that of powered antenna coil, as shown in Sections III-B and C. The depth of the chamber affects nonuniformity, the position of maximum density, and electron temperature because of the transport of energetic electrons and diffusion of the bulk plasma. The effect is more profound than that of the inductively coupled plasma chamber with external antenna coils. As a result, we obtain good uniformity (nonuniformity 3.1%) at $1020 \times 830 \times 300$ mm. In the future, in order to find more parameter affecting the plasma uniformity in this chamber, we will consider the voltage distribution obtained from experiment and use permanent magnet. The optimized condition for good uniformity will be applied to the experiment of our coworker.

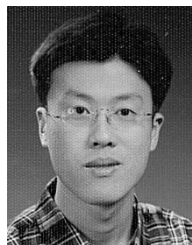
REFERENCES

- [1] Y. Wu and M. A. Lieberman, "The influence of antenna configuration and standing wave effects on density profile in a large-area inductive plasma source," *Plasma Source Sci. Technol.*, vol. 9, pp. 210–218, 2000.
- [2] K. Takechi and M. A. Lieberman, "Photoresist etching in an inductively coupled, traveling wave driven, large area plasma source," *J. Appl. Phys.*, vol. 89, pp. 869–877, 2001.
- [3] —, "Effect of Ar addition to an O₂ plasma in an inductively coupled, traveling wave driven, large area plasma source O₂/Ar mixture plasma modeling and photoresist etching," *J. Appl. Phys.*, vol. 90, pp. 3205–3211, 2001.
- [4] R. A. Stewart, P. Vitello, and D. B. Graves, "Two-dimensional fluid model of high density inductively coupled plasma source," *J. Vac. Sci. Technol., B*, vol. 12, pp. 478–485, 1994.
- [5] R. A. Stewart, P. Vitello, D. B. Graves, E. F. Jaeger, and L. A. Berry, "Plasma uniformity in high-density inductively coupled plasma tools," *Plasma Source Sci. Technol.*, vol. 4, pp. 36–46, 1995.
- [6] J. D. Bukowski and D. B. Graves, "Two-dimensional fluid model of an inductively coupled plasma with comparison to experimental spatial profiles," *J. Appl. Phys.*, vol. 80, pp. 2614–2623, 1996.
- [7] P. L. G. Ventzek, R. J. Hoeksta, and M. J. Kushner, "Two-dimensional modeling of high plasma density inductively coupled sources for materials processing," *J. Vac. Sci. Technol. B*, vol. 12, pp. 461–477, 1994.
- [8] S. Raul and M. J. Kushner, "Model for noncollisional heating inductively coupled plasma source processing source," *J. Appl. Phys.*, vol. 81, pp. 5966–5974, 1997.
- [9] H. C. Kim, M. S. Hur, S. S. Yang, S. W. Shin, and J. K. Lee, "Three-dimensional fluid simulation of a plasma display panel cell," *J. Appl. Phys.*, vol. 91, pp. 9513–9520, 2002.
- [10] J. K. Lee, L. Meng, Y. K. Shin, H. J. Lee, and T. H. Chung, "Modeling and simulation of a large-area plasma source," *Jpn. J. Appl. Phys.*, vol. 36, pp. 5714–5723, 1997.
- [11] Y. K. Shin, C. H. Shon, W. Kim, and J. K. Lee, "The voltage-pulsing effects in AC plasma display panel," *IEEE Trans. Plasma Sci.*, vol. 27, pp. 1366–1371, Oct. 1999.
- [12] J. Meunier, P. Beenguer, and J. P. Boeuf, "Numerical model of an ac plasma display panel cell in neon-xenon mixtures," *J. Appl. Phys.*, vol. 78, pp. 731–745, 1995.
- [13] J. P. Boeuf and L. C. Pitchford, "Pseudospark discharge via computer simulation," *IEEE Trans. Plasma Sci.*, vol. 19, pp. 286–296, Apr. 1991.
- [14] D. L. Sharfetter and H. K. Gummel, "Large-signal analysis of a silicon read diode oscillator," *IEEE Trans. Electron Devices*, vol. 16, p. ED-64, Jan. 1967.
- [15] J. Douglas and J. E. Gunn, "A general formulation of alternating direction methods—Part I. Parabolic and hyperbolic problems," *Numer. Math.*, vol. 6, pp. 428–453, 1964.
- [16] T. H. Chung, L. Meng, H. J. Yoon, and J. K. Lee, "Two-dimensional fluid simulation of capacitively coupled RF electronegative plasmas," *Jpn. J. Appl. Phys.*, vol. 36, pp. 2874–2882, 1997.
- [17] M. A. Lieberman and A. J. Lichtenberg, *Principles of Plasma Discharges and Materials Processing*. New York: Wiley, 1994, ch. 12, pp. 396–398.
- [18] J. A. Stittsworth and A. E. Wendt, "Reactor geometry and plasma uniformity in a planar inductively coupled radio frequency argon discharge," *Plasma Source Sci. Technol.*, vol. 5, pp. 429–435, 1996.
- [19] U. Kortshagen and B. G. Heil, "Kinetic two-dimensional modeling of inductively coupled plasmas based on a hybrid kinetic approach," *IEEE Trans. Plasma Sci.*, vol. 27, pp. 1297–1309, Oct. 1999.
- [20] F. F. Chen, J. D. Evans, and G. R. Tynan, "Design and performance of distributed helicon sources," *Plasma Source Sci. Technol.*, vol. 10, pp. 236–249, 2001.
- [21] W. M. Manheimer, R. F. Fernsler, M. Lampe, and R. A. Meger, "Theoretical overview of the large-area plasma processing system," *Plasma Source Sci. Technol.*, vol. 9, pp. 370–386, 2000.
- [22] H. M. Wu, "Two-dimensional hybrid model simulation and validation for radio frequency inductively coupled oxygen plasma," *Plasma Source Sci. Technol.*, vol. 9, pp. 347–352, 2000.
- [23] M. Li, H. M. Wu, and Y. Chen, "Two-dimensional simulation of inductive plasma sources with self-consistent power deposition," *IEEE Trans. Plasma Sci.*, vol. 23, pp. 558–562, Aug. 1995.
- [24] T. Makabe and N. Nakano, "Modeling and diagnostics of the structure of rf glow discharges in Ar at 13.56 MHz," *Phys. Rev. A, Gen. Phys.*, vol. 45, pp. 2520–2530, 1992.
- [25] K. Kamimura, K. Iyanagi, N. Nakano, and T. Makabe, "Two-dimensional modeling of spatiotemporal structure of inductively coupled plasma," *Jpn. J. Appl. Phys.*, vol. 38, pp. 4429–4435, 1999.



Sea Eun Park was born in Daegu, South Korea, in 1975. He received the B.S. degree in electronics engineering from Kyungbuk National University, Daegu, South Korea, in 2001 and the M.S. degree in electronic and electrical engineering from the Pohang University of Science and Technology, Pohang, South Korea, in 2003.

He is currently with Hynix Semiconductor Company, Gyeonggi, South Korea. His research interests include the inductively coupled plasma source and the large area plasma source simulation.



Byung Ug Cho was born in Chungju, South Korea, in 1977. He received the B.S. degree in electronics engineering from Chungbuk National University, Chungju, South Korea, in 2002. He is currently working toward the M.S. degree at Pohang University of Science and Technology, Pohang, South Korea.

His current research interests include the inductively coupled plasma source and the large area plasma source simulation.



Jae Koo Lee (M'83) received the Ph.D. degree from the University of California, Berkeley, in 1979.

From 1979 to 1989, he was a Senior (later a Staff) Scientist on tokamak theory with General Atomics, San Diego, CA. He is currently a Professor in the Department of Electronic and Electrical Engineering, Pohang University of Science and Technology, Pohang, South Korea. He is currently on the Editorial Board of *Plasma Source and Science and Technology*. His research interests include the theory and simulation of low-temperature basic-processing plasmas, fusion plasmas, and free-electron lasers.

Dr. Lee is the past Chair of Division of Plasma Physics of Korean Physical Society.



Young Joon Lee was born in Seoul, South Korea, in 1972. He received the B.S. and M.S. degrees in materials science and engineering from Sungkyunkwan University (SKKU), Gyeonggi, South Korea, in 1996 and 1998, respectively. He is currently working toward the Ph.D. degree at SKKU.

His research interests include the plasma etching process development and the large area plasma source development.



Geun Young Yeom received the Ph.D. degree in electronic materials engineering from the University of Illinois, Urbana-Champaign, in 1989.

From 1989 to 1991, he was with Tektronics Inc., Beaverton, OR, where he worked in a process development position on developing etching processes for a bipolar IC. From 1991 to 1992, he was with Silicon Systems, Tustin, CA. In 1992, he became a Professor with the Materials Science and Engineering Department, Sungkyunkwan University, Gyeonggi, South Korea. His current research interests include

the development of equipments and processes related to plasma etching.